Adjustment of a turbulent boundary layer to a canopy of roughness elements

By S. E. BELCHER[1], N. JERRAM†[2] AND J. C. R. HUNT[3]

[1]Department of Meteorology, PO Box 243, University of Reading, Reading, RG6 6BB, UK

[2]Department of Applied Mathematics and Theoretical Physics, University of Cambridge, Centre for Mathematical Sciences, Wilberforce Road, Cambridge, CB3 0WA, UK

[3]Department of Space and Climate Physics, University College, Gower Street, London, UK

A model is developed for the adjustment of the spatially averaged time-mean flow of a deep turbulent boundary layer over small roughness elements to a canopy of larger three-dimensional roughness elements. Scaling arguments identify three stages of the adjustment. First, the drag and the finite volumes of the canopy elements decelerate air parcels; the associated pressure gradient decelerates the flow within an *impact region* upwind of the canopy. Secondly, within an *adjustment region* of length of order L_c downwind of the leading edge of the canopy, the flow within the canopy decelerates substantially until it comes into a local balance between downward transport of momentum by turbulent stresses and removal of momentum by the drag of the canopy elements. The adjustment length, L_c, is proportional to (i) the reciprocal of the roughness density (defined to be the frontal area of canopy elements per unit floor area) and (ii) the drag coefficient of individual canopy elements. Further downstream, within a *roughness-change region*, the canopy is shown to affect the flow above as if it were a change in roughness length, leading to the development of an internal boundary layer. A quantitative model for the adjustment of the flow is developed by calculating analytically small perturbations to a logarithmic turbulent velocity profile induced by the drag due to a sparse canopy with $L/L_c \ll 1$, where L is the length of the canopy. These linearized solutions are then evaluated numerically with a nonlinear correction to account for the drag varying with the velocity. A further correction is derived to account for the finite volume of the canopy elements. The calculations are shown to agree with experimental measurements in a fine-scale vegetation canopy, when the drag is more important than the finite volume effects, and a canopy of coarse-scale cuboids, when the finite volume effects are of comparable importance to the drag in the impact region. An expression is derived showing how the effective roughness length of the canopy, z_0^{eff}, is related to the drag in the canopy. The value of z_0^{eff} varies smoothly with fetch through the adjustment region from the roughness length of the upstream surface to the equilibrium roughness length of the canopy. Hence, the analysis shows how to resolve the unphysical flow singularities obtained with previous models of flow over sudden changes in surface roughness.

1. Introduction

The surfaces of the Earth and oceans are covered with roughness elements, such as grass or bushes over land, or ripples and waves on the ocean. When the roughness

† Present address: Data Connection Ltd, Enfield, UK.

elements are small, it is conventional to consider only the flow over the roughness elements. However, when the roughness elements are larger, such as crops or buildings, it is often necessary to know details of the flow between the roughness elements as well as the flow over the group of roughness elements. It is then appropriate to think of the group of roughness elements as a *canopy*. Despite progress in the past few years in the use of the roughness length to parameterize effects of varying surface roughness, better modelling is needed, particularly for the non-uniform region in the vicinity of the roughness change, in order to tackle practical problems such as mesoscale numerical weather prediction and air quality forecasting in urban areas and hilly terrain, which then determine climatic and agricultural effects of air movements and fluxes in and out of these canopies.

The overall effects of a canopy of roughness elements on the turbulent flow that passes over them are usually parameterized as a roughness length, z_0^{eff}. Such a parameterization is compact and effective in many applications, but has limitations. First, this method gives no information about the flow between the roughness elements themselves, which is required for modelling scalar transport in applications of urban air quality and dispersion in agricultural crops. Secondly, there is at present no general systematic method for obtaining the roughness length from the geometry of the roughness elements and their spatial distribution. Indeed, Grimmond & Oke (1999) have shown that the methods in current use cannot even explain satisfactorarily the flow over symmetrically distributed roughness elements of the same size, let alone those over typical non-uniform non-symmetrically distributed obstacles found in practice. Thirdly, the roughness length is only defined when the wind profile above the roughness elements is logarithmic. Hence, when the flow above the area of roughness elements is accelerating or decelerating it is not even clear whether or not the roughness length can be defined (Krettenauer & Schumann 1992). Finally, representing a change in the density or type of surface roughness elements by a change in their roughness lengths, z_0, leads to unrealistically large changes in shear stress at the upwind edge of a change (e.g. Belcher, Xu & Hunt 1990). The object of this paper is to develop understanding and quantitative modelling of these complex boundary-layer flows, and to suggest how to improve the use of the roughness length as a practical parameterization.

These problems are addressed here with a more refined treatment of the effects of the roughness elements on the flow. The calculations are based on the approximations, first, that the volume occupied by the canopy acts as a region of drag on the wind (see for example Kaimal & Finnigan 1995, chapter 3) and, secondly, that the finite volumes of the roughness elements of the canopy displace the flow. As noted by Finnigan (2000), previous work has focused on the conditions when the boundary layer is fully adjusted to the canopy, such as over large areas of vegetation. Here, since we are motivated particularly by winds over and within urban areas whose building densities are often inhomogeneous, we focus specifically on the adjustment of the boundary-layer flow as it approaches and passes over the canopy elements.

There are several fluid dynamical questions that need to be answered. First, how does the boundary-layer flow above the canopy adjust to the flow within it? In particular, is the flow just above the canopy equivalent to that over a change in roughness with a logarithmic boundary-layer profile displaced upwards a distance d (as suggested by the measurements of Rotach, 1993, over the city of Zurich). Secondly, what are the effects of the various dynamical processes in these complex boundary-layer flows? The processes include blocking of boundary-layer eddies by
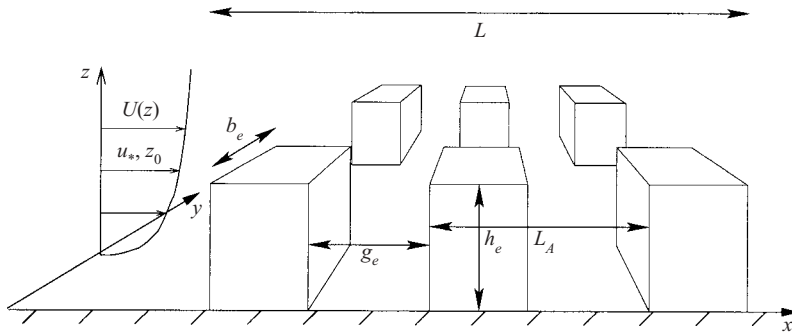
FIGURE 1. Geometry of the canopy elements and the approach flow.

the shear layer that forms at the top of the canopy (Hunt & Durbin 1999), and interaction between the boundary layer and canopy flows through eddies generated by a mixing-layer instability at the top of the canopy (Raupach, Finnigan & Brunet 1996). A third question, therefore, is whether a simple mixing length parameterization may be valid over part of the flow, as found in studies of flow over roughness changes (Belcher *et al.* 1990) and studies of the mean wind profile within a vegetation canopy (Wilson, Finnigan & Raupach 1998). Fourthly, as in flow over roughness changes (Townsend 1976) and two-phase flows (Kowe *et al.* 1988), the effects of the obstacles on the flow are modelled in an averaged sense over an area or volume occupied by many obstacles and by introducing an extra shear stress or body force into the momentum equations, rather than calculating the flow around each obstacle. Can these factors be defined in terms of simple properties of the roughness elements and the surface? These questions are addressed in this paper.

In §2, a model for boundary-layer flow through groups of obstacles is formulated by representing the obstacles as a canopy with a drag on the wind. In §2.1, a simple method is developed to estimate the mean drag exerted by the canopy on the mean flow in terms of properties of the canopy elements, with an analysis of the characteristic scales of flow and the flow perturbations in a homogeneous canopy. Depending on the density of the canopy, two different models for turbulent momentum transport within the canopy are developed in §2.2. The characteristics and scalings for how the boundary layer adjusts to the canopy are described in §3. The method of solving the resulting equations is described in §4. Comparisons of the model with previous computations and with measurements made both in the field and in the wind tunnel are shown in §5. Section 6 describes the variation of the effective roughness length of the canopy with distance through the canopy. Conclusions are given in §7.

2. Development of idealized models

A fully developed atmospheric boundary layer, with wind components $U_0 = (U_0(z), 0, 0)$, blows in the positive x-direction, with the z-axis pointing upwards vertically, see figure 1. Here, we consider the changes to this boundary layer as it impinges upon a canopy, composed of a group of many solid roughness elements. To fix ideas, think of a canopy that extends over a length L and formed by N_e elements, with typical height h_e, breadth b_e, and gap between canopy elements g_e.

The canopy elements have two effects on the mean flow. First, the body force associated with the pressure drop across individual elements exerts a drag that

decelerates the mean flow. Secondly, the displacement of streamlines around individual canopy elements can also transports momentum. The aim here is to calculate the main effect of the canopy of obstacles by computing the spatially averaged time-mean flow, called here the mean flow. In this way, we compute the evolution of the flow as the canopy density varies, but avoid calculating the details of the flow around individual canopy elements. The spatial average is taken over a horizontal area with side of length L_A. For a periodic array of obstacles, L_A is the length of the repeating unit. For a random array, L_A encompasses several obstacles, such that L_A is much greater than the gap between individual obstacles but much less than the length scale over which the mean obstacle density changes. This approach was initiated by Taylor (1944), see Batchelor (1967, §5.15), and has been further developed for flows in vegetation canopies, see Finnigan (2000).

Consider, for simplicity, the case when the fraction of the canopy volume occupied by obstacles, β, is small, i.e. the gap between the elements g_e is large compared with their breadth b_e, $\beta \sim b_e^2/g_e^2 \ll 1$. The aerodynamic drag of the obstacles, which remains substantial, can then be represented by a point force at the centre of each roughness element. The spatial averaging operation renders these point forces into a continuous resistive body force that extends throughout the canopy volume. In addition, the displacement of streamlines by individual canopy elements yields, on averaging spatially, a net momentum transport, the *dispersive stress* described by Raupach & Shaw (1982) and Finnigan (1985). There is experimental evidence (Finnigan 1985; Cheng & Castro 2002a) that near the top of the canopy the dispersive stress is very small compared to the Reynolds stress. The dispersive stress may be a larger fraction near the bottom of the canopy (Bohm, Finnigan & Raupach 2000), but both stresses tend to be small there. Hence, as we shall see, the drag term is important through the whole volume of the canopy, whereas the dispersive stress can be neglected; although we shall see that the finite volumes of the canopy elements lead to a dispersive stress that is important upwind of the canopy.

We begin by analysing the effect of the drag term on the flow. Hence, on ignoring the dispersive stress, the equations governing the spatially averaged time-mean flow are

$$U_j \frac{\partial U_i}{\partial x_j} + \frac{\partial P}{\partial x_i} = \frac{\partial \tau_{ij}}{\partial x_j} - f_i, \tag{2.1}$$

$$\frac{\partial U_i}{\partial x_i} = 0. \tag{2.2}$$

Hereinafter, $x_i = (x, y, z)$ and $\tau_{13} = \tau$, and the pressure, stress and drag force are defined such that the density is one throughout. The model is completed on parameterizing the spatially averaged turbulent stress, τ_{ij}, and drag per unit volume, f_i. These aspects are considered next.

2.1. *Relating the obstacle drag to the flow*

First, the drag per unit volume, f_i, is related to the spatially averaged time-mean flow, $U(x, y, z)$, referred to here as the mean flow. Consider the drag on a test canopy element, defined in analogy with the test charge in electrodynamics. The drag on the test element is associated with a momentum deficit in the wake of the element that spreads throughout the fluid in the canopy volume and thus slows the mean flow. Similarly, the mean flow impinging upon the test element is reduced by the presence of the other canopy elements and is measured by the spatially averaged time-mean

flow speed, $U(x, y, z)$. Since the Reynolds number of the flow around the test element is large, the drag varies as the square of the impinging wind speed (Batchelor 1967, §5.11). The drag on the test element then scales as U^2 and is reduced by the presence of the other canopy elements (cf. Wood & Mason 1993). These arguments suggest that the drag on each canopy element scales on U^2 multiplied by a factor that is independent of U. The spatial averaging smoothes these point forces to yield f_i, the drag per unit volume of canopy. Hence, on dimensional grounds, f_i can be expressed as the ratio of U^2 and a *canopy-drag length scale*, L_c, namely

$$f_i(\boldsymbol{x}) = \frac{|\boldsymbol{U}|U_i}{L_c}, \qquad (2.3)$$

with L_c independent of U. The drag $f_i = 0$ outside the canopy.

Explicit estimates for L_c are now obtained for illustration by considering an array of N_e tall slender canopy elements, each with breadth b_e and frontal area $A_f \sim h_e b_e$, and covering a total floor area A_t. At height z, the *sectional drag coefficient*, $c_d(z)$, is defined, following MacDonald (2000), to be the drag at height z divided by half the square of the spatially averaged time-mean wind at that height, $U^2(z)/2$, multiplied by the frontal width (per unit floor area) presented to the flow by the obstacles, i.e. $N_e b_e/A_t$. The force per unit volume acting at height z is then $(N_e b_e/A_t)c_d(z)U^2(z)/2$. When the obstacles have a uniform horizontal cross-section, the height and breadth can be related to the frontal area through $b_e = A_f/h_e$. MacDonald (2000) shows how this expression is related to a conventional (depth integrated) expression for the drag and drag coefficient.

Now, this drag of the canopy decelerates the fluid within the canopy and hence acts only within the fraction of volume occupied by fluid, $(1 - \beta)$. Hence, the drag is divided by a factor of $(1 - \beta)$. As β increases, this process becomes more important and is considered by Eames, Hunt & Belcher (2003). Taken together, for this illustrative case, there is an average force per unit volume acting on the fluid within the canopy of $U^2 N_e \bar{c}_d A_f/2(1 - \beta)h_e A_t$ (where $\bar{c}_d$ is the average sectional drag coefficient), so that the average canopy-drag length scale L_c is given by

$$\frac{1}{L_c} = \frac{N_e \frac{1}{2}\bar{c}_d A_f}{(1 - \beta)h_e A_t} = \frac{\frac{1}{2}\bar{c}_d \lambda}{(1 - \beta)h_e} \sim b_e/g_e^2, \qquad (2.4)$$

where $\lambda = N_e A_f/A_t \sim h_e b_e/g_e^2$ is the *roughness density* (see also Wooding, Bradley & Marshall 1973; Raupach 1992). We note that the coefficient $N_e A_f/h_e A_t$ is equivalent to the leaf area index, a, with units of m^{-1}, referred to in the literature on forests and plant canopies (e.g. Kaimal & Finnigan 1995, p. 79).

The model just developed is sufficiently flexible to account for inhomogeneous canopies. When the characteristics of the canopy elements vary in space, as they do through an urban area, the canopy length scale, L_c, also varies. Formally, this variation must be on length scales greater than the averaging length scale L_A.

2.2. *Models for the turbulent stress*

Hunt *et al.* (2001) show that the dynamics of turbulence are approximately local, so that the turbulent stress is approximated by Prandtl's mixing-length model, when (i) the distortion time scale T_d at which the mean shear and strain change along the trajectories of fluid elements is comparable with or larger than the Lagrangian timescale of the energy containing eddies and (ii) the integral length scale L_x of the eddies is no larger than the length scales over which the mean shear changes, i.e. $L_x \leqslant |dU/dz|/|d^2U/dz^2|$. A shear layer develops at the top of a homogeneous
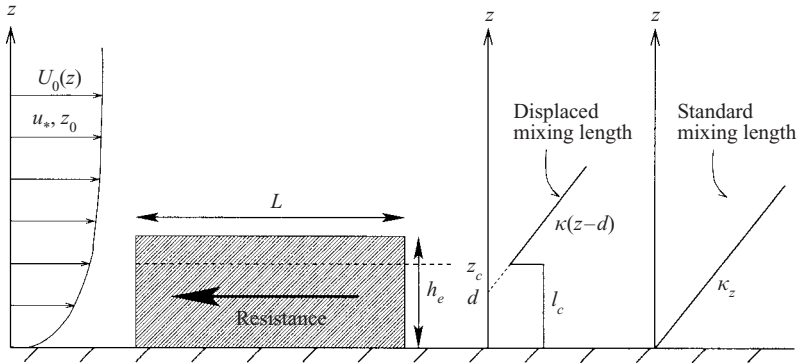
FIGURE 2. Geometry of the canopy and two models for the mixing-length.

canopy and generates mixing-layer-type eddies (Raupach *et al.* 1986), which satisfy these conditions only marginally. Hence, for homogeneous canopies, the mixing-length model has limitations (Raupach *et al.* 1996). Nevertheless, for the perturbed canopy flows considered here, the mixing-length model can be justified as the first term in an expansion (Finnigan & Belcher 2003). Hence, we adopt the mixing-length model here.

In the boundary-layer analysis developed here, the vertical gradient of the shear stress, $\partial\tau/\partial z$, is the dominant Reynolds stress gradient in the mean momentum budget, which, with the mixing-length model, has the general form

$$\frac{\partial\tau}{\partial z} = \frac{\partial}{\partial z}\left\{l_m^2\left(\frac{\partial U}{\partial z}\right)^2\right\}. \tag{2.5}$$

Even in the limit of $\beta \ll 1$, it is helpful to consider how the turbulence structure changes as the canopy increases in density. If the canopy is extremely sparse, then the structure of the turbulence in the approaching boundary layer is not much changed by the canopy. The length scale of the eddies that determine the dissipation rate is then unchanged, i.e.

$$l_m \approx \kappa z, \tag{2.6}$$

where $\kappa = 0.4$ is the von Kármán constant (see figure 2). This approximation has been used in selected regions of other perturbed turbulent boundary layers such as flow over changing surface roughness (Belcher *et al.* 1990) and flow over elevation changes (Belcher, Newley & Hunt 1993). We denote as *very sparse canopies* those canopies where the surface shear stress is not significantly affected by the canopy, i.e. $f \ll \mathrm{d}\tau/\mathrm{d}z$ so that

$$\lambda \sim \beta\frac{h_e}{b_e} \ll \frac{u_*^2}{U_h^2} \sim \left\{\frac{\kappa}{\ln(h_e/z_0)}\right\}^2 \sim 0.1-0.01. \tag{2.7}$$

The mixing length can then be approximated by (2.6).

When $b_e u_*^2/h_e U_h^2 \ll \beta \ll 1$, the canopy is still sparse enough that the mean flow perturbation is small, but dense enough that the turbulence is affected by the drag of the canopy, both indirectly by the drag changing the mean flow and directly by the drag acting on the eddies themselves (Finnigan 2000). In this regime, the distribution of mean shear in a canopy that is homogeneous in the streamwise direction is determined by downward transport of momentum by turbulent stresses balancing
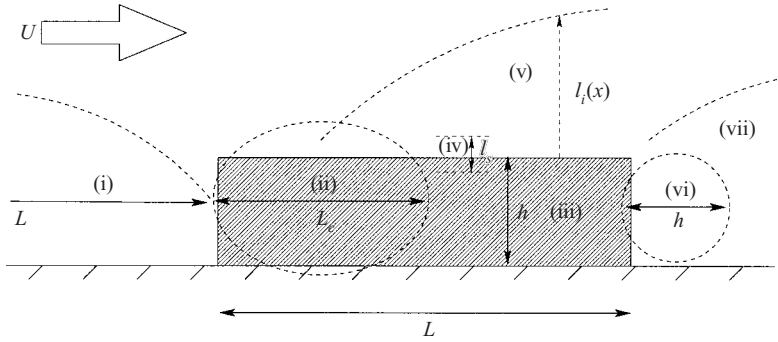
FIGURE 3. Characteristics of the adjustment to the canopy. (i) Impact region; (ii) adjustment region (iii) canopy interior; (iv) canopy shear layer; (v) roughness-change region; (vi) exit region; (vii) far wake.

removal of momentum by canopy drag (region (iii) in figure 3). Then from (2.1), (2.3) and (2.5) the mean momentum equation reduces to

$$0 = \frac{\mathrm{d}}{\mathrm{d}z}\left\{ l_m^2 \left(\frac{\mathrm{d}U}{\mathrm{d}z}\right)^2 \right\} - \frac{U^2(z)}{L_c(z)}. \tag{2.8}$$

The horizontal wind speed within the canopy, $U(z)$, decays with depth from the top of the canopy, where it is U_h, to a very low value within a layer of depth l_s, which can be estimated from (2.8). The turbulent stress gradient is then of the order

$$\frac{\mathrm{d}}{\mathrm{d}z}\left\{ l_m^2 \left(\frac{\mathrm{d}U}{\mathrm{d}z}\right)^2 \right\} \sim \frac{1}{l_s}\left\{ l_m^2 \left(\frac{U_h}{l_s}\right)^2 \right\}, \tag{2.9}$$

and the canopy drag scales as $U^2/L_c \sim U_h^2/L_c$, so equations (2.8) and (2.9) yield

$$l_s \sim \left(l_m^2 L_c\right)^{1/3} \qquad \text{so that} \qquad l_s/h_e \sim (l_m/h_e)^{2/3}(L_c/h_e)^{1/3}. \tag{2.10}$$

Hence, l_s is controlled partly by the mixing length l_m, which determines the efficiency of the turbulence to mix momentum down into the canopy, and partly by the canopy-drag length scale L_c, which determines the efficiency of the canopy to remove momentum.

Now, increasing the canopy element density increases the canopy drag, and so tends to decrease L_c. In addition, the wake turbulence generated by the additional canopy elements leads to an enhanced rate of turbulence dissipation (Ayotte, Finnigan & Raupach 1999), which tends to reduce the mixing length l_m. From (2.10), these two tendences both tend to reduce l_s and increase the mean shear which has two effects on the turbulence:

First, vorticity within this shear layer fluctuates in response to vorticity associated with large boundary-layer eddies above the canopy. This *shear sheltering* (Hunt & Durbin 1999) tends to block the large boundary-layer eddies, which explains why, in measurements above urban areas (e.g. Rotach 1993), the eddy scales for vertical transport, and hence also the mixing length, increase linearly from the blocking shear layer, i.e.

$$l_m = \kappa(z - d) \qquad \text{when } z > d. \tag{2.11}$$

Here, d is the displacement height. This analysis explains why the displacement height lies within the shear layer at the top of the canopy, as observed by Thom

(1971) and proposed by Jackson (1981). The measurements of Rotach (1993) and Raupach, Thom & Edwards (1980) suggest that this mechanism operates even when the canopy consists of obstacles with finite aspect ratios ($h_e \sim b_e$), so that there are large recirculations in the wakes of the canopy elements. Canopies dense enough that the turbulence structure is changed from the form (2.6) for very sparse canopies, to either of the forms (2.12) or (2.13) we refer to as *dense canopies*.

Secondly, the shear layer at the top of the canopy is itself dynamically unstable (as observed by Louka, Belcher & Harrison 2000) and produces turbulent eddies characteristic of free shear layers, whose length scales are about equal to the thickness of the shear layer (Raupach *et al.* 1996; Finnigan 2000). Finnigan & Brunet (1995) show that the shear-layer motions are only weakly coupled to the large-scale boundary-layer eddies above the canopy, in agreement with the idea of shear sheltering. The movement of these inhomogeneous and non-Gaussian eddies down into the canopy mean that these shear layer motions provide much of the energy of the turbulence through the depth of the canopy (Finnigan 2000). Thus, within the canopy, the mixing length, l_m, scales on the size of these shear-layer eddies and is approximately constant, say $l_m = l_c$, with height.

If the canopy consists of roughness elements of approximately uniform dimensions or if the canopy consists of roughness elements whose breadths, b_e, are much smaller than the thickness of the shear layer, i.e. $b_e \ll l_s$, then the mixing length, l_m, is constant with height and proportional to the thickness of the shear layer, i.e.

$$l_m = l_c \propto l_s \quad \text{when } z < d. \tag{2.12}$$

Canopies consisting of roughness elements of highly irregular shapes induce large vortical wakes that interact with the downstream elements (e.g. Britter & Hunt 1979). The mean spatially averaged shear layer then ceases to control the dynamics of the turbulence. Instead, the mixing length is controlled by the vortices shed in the obstacle wakes, which are of order h_e:

$$l_c \propto h_e. \tag{2.13}$$

This value is very much greater than the value in the turbulent boundary layer above the canopy, where $l_m = \kappa(z - d)$. The wind shear is then much smaller within the canopy, so that the wind profile is more uniform with height.

At the bottom of the canopy, very close to the ground, the eddies are blocked by the ground, so that, as in turbulence near any plane surface,

$$l_m = \kappa z. \tag{2.14}$$

For a dense deep canopy, where $h_e \gg l_s$, Inoue (1963) has shown that the solution to (2.9) is

$$U = U_h \exp\left((z - h_e)/l_s\right), \tag{2.15}$$

with $l_s = (2l_c^2 L_c)^{1/3}$, which confirms the scaling (2.10) for this particular case.

For a finite-depth canopy, where $h_e \leqslant l_s$, the exponential solution is approximately valid in the upper portion of the canopy. However, near the ground, where $\kappa z < l_c$, the wind speed is small, i.e. $U^2/L_c \ll d\tau/dz$, so that the mean wind profile is close to a classical logarithmic form. The wind speed near the ground can then be estimated to be

$$U(0) \approx U_h \exp\left(-h_e/l_s\right). \tag{2.16}$$

This leads to the useful distinction between of *shallow canopies* where $l_s/h_e = (l_c/h_e)^{2/3}(L_c/h_e)^{1/3} \sim 1$ and *deep canopies* which have $l_s/h_e \ll 1$. For irregular canopies,

with larger $l_c \sim h_e$, the average wind profile is more uniform with height, whence (2.16) shows how the surface winds are higher. Urban canopies tend to be shallow, whereas vegetation canopies tend to be deep.

Given these arguments, two models are used here to parameterize the mixing length in the analysis of adjustment to a canopy, see figure 2. First, for very sparse canopies we use the *standard mixing-length model*, which increases linearly from the ground according to (2.6). Secondly, for dense canopies we use the *displaced mixing-length model*, which is constant within the canopy and then increases linearly with height above the shear layer at the top of the canopy, namely

$$l_m = l_c \quad \text{when } z < z_c,$$
$$l_m = \kappa(z - d) \quad \text{when } z > z_c. \tag{2.17}$$

The region close to the ground in the dense canopies is neglected in the present study.

3. Characteristics of adjustment of the boundary layer to a canopy

Before developing a quantitative model for the adjustment of the boundary layer to a canopy, scaling arguments are developed to show the characteristics of the adjustment and to interpret the quantitative results obtained in §4 below for the linearized model. The adjustment is found to proceed through distinct regions, which are shown schematically in figure 3. The controlling dynamics of these regions and their magnitudes are estimated from the momentum equations.

The drag of the canopy elements acts as an impulse decelerating air parcels, which increases the mean pressure within the canopy. Hence, there is a pressure gradient that decelerates the flow within an *impact region* that extends upwind of the canopy, denoted (i) in figure 3. By continuity, the deceleration of the streamwise flow leads to a vertical motion over and out of the canopy. This mean vertical motion transports fluid upwards, and may be greater than vertical transport of momentum by turbulence in regions (i) and (ii).

From the leading edge of the canopy, within an *adjustment region*, denoted (ii) in figure 3, the wind within the canopy is decelerated by the canopy drag. The deceleration is largely inviscid and so the canopy drag is largely balanced by streamwise advection. The streamwise lengthscale of the adjustment region can therefore be estimated by balancing the nonlinear drag with the nonlinear streamwise advection, namely

$$U \frac{\partial U}{\partial x} \sim \frac{U^2}{L_c}. \tag{3.1}$$

The kinetic energy in the mean streamwise velocity, $U^2/2$, is therefore reduced approximately exponentially on a lengthscale $L_c/2$ (cf. Finnigan & Brunet 1995). Thus, the canopy lengthscale, L_c, represents the streamwise distance required for the canopy to rob an air parcel of its kinetic energy, and hence gives an estimate for the distance for the winds within the canopy to adjust. Deceleration of the streamwise velocity leads, by continuity, to a vertical flux out of the top of the canopy within this adjustment region. Meanwhile, turbulent stresses transport momentum downwards into the canopy.

Further downwind, the local balance given in equation (2.8) is achieved, with the loss of momentum by canopy drag balancing the downward transport of momentum by turbulent stresses. The flow within the canopy has then adjusted. This is the *canopy interior flow*, denoted by (iii) in figure 3. Here, the velocity profile is given by (2.15)

and (2.16). As described in § 2.2, there is a layer of shear of thickness l_s between the canopy flow and the boundary-layer flow above, denoted (iv) in figure 3. The spatially averaged flow above the canopy requires separate consideration with the effect of the canopy being represented by an effective roughness length, z_0^{eff}. An internal boundary layer develops in region (v) above the canopy, $z > h_e$. Its depth, $l_i(x)$, is determined, following Townsend (1965), by balancing streamwise advection and vertical transport by the turbulent stress to yield

$$l_i \ln \left(l_i / z_0^{eff} \right) \approx 2\kappa^2 (x - x_0). \tag{3.2}$$

Notice how the canopy affects l_i through the effective roughness length, z_0^{eff}, and through the effective origin, x_0. At the effective origin for this internal boundary layer, x_0, there is a smooth transition from vertical transport driven by the mean velocity out of the canopy, $w(z = h_e) \sim U_h(h_e/L_c)\exp(-x/L_c)$, to that driven by the vertical transport by turbulence. Hence, we identify $x = x_0$ where $w(z = h_e) \sim u_*$. It follows that

$$x_0 \sim L_c \ln \left\{ \left(\frac{U_h}{u_*} \right) \left(\frac{h_e}{L_c} \right) \right\}. \tag{3.3}$$

Thus, there is a smooth transition a distance of order x_0 downstream of the canopy edge. If the canopy is exceptionally long, the boundary layer above may fully adjust to the effective roughness of the canopy.

Just above the canopy elements, within the roughness sublayer, there are also time-averaged motions associated with the flow around individual roughness elements. Point measurements (rather than spatially averaged measurements) yield the internal boundary-layer structure only when l_i has grown higher than the roughness sublayer, which typically has depth 2–$3h_e$ (e.g. Rotach 1993; Louka *et al.* 2000). Cheng & Castro (2002*b*) have shown how this occurs considerably downstream of the leading edge of the canopy. Nevertheless, these complications of the roughness sublayer are avoided when the spatially averaged flow is considered, as it is here.

In the vicinity of the downstream edge of the array is the *exit region*, denoted (vi) in figure 3. Here, the resistance of the canopy suddenly disappears. There is therefore a force imbalance on the mean flow below h_e and the mean wind accelerates, leading, by continuity, to a downwards mean vertical velocity. Turbulent stresses transport further momentum downwards to fill the velocity deficit in the wake over a streamwise length scale of order $h_e U_h/u_*$.

Yet further downstream is the *far wake region*, denoted (vii) in figure 3, where the dynamics is dominated by streamwise advection and downward momentum transport by turbulent stresses. The flow develops in a similar way to the wake behind a single bluff obstacle on a surface. Hence, the wake-velocity deficit, Δu, is expected to develop as $\Delta u \propto h_e U_h/x$, and the height of the wake, $h_w(x)$, increases approximately as $h_w \propto (x h_e)^{1/2}$ (Counihan, Hunt & Jackson 1974). Sufficiently far downstream, the boundary layer returns to its far upstream profile.

4. A linear model for adjustment to a canopy

We now develop an analysis of the linear changes to the spatially averaged flow as a turbulent boundary layer passes through a distributed force, which shows how the regions analysed in § 3 match each other and confirms the order of magnitude estimates. The description given here is approximate. (Jerram 1995, chapter 3, gives full details of a formal matched asymptotic analysis. A copy of this analysis is

available from the JFM office.) The force distribution is localized around the origin of coordinates and varies over a characteristic horizontal length scale L and maximum height h_e (see figure 2). The incident wind profile is logarithmic with roughness length z_0 and friction velocity u_*. In the following analysis, we calculate changes to the boundary layer induced by a *weak canopy*, $L/L_c \ll 1$, so that changes to the boundary layer are small and therefore can be calculated from the linearized momentum equations. Subsequently, these linear solutions are iterated numerically to obtain changes for denser canopies.

4.1. *Governing equations*

Each physical quantity, for example the spatially averaged velocity components, U_i, pressure, P, and stress tensor, τ_{ij}, is written as the sum of the incident profile, which would exist in the absence of any canopy and which is denoted by subscript 0, and a perturbation part induced by the canopy, which is denoted by lower case letters. The streamwise velocity component, for example, is then written $U = U_0 + u$. The equations are then linearized for small perturbations by neglecting products of perturbation quantities. On retaining only the dominant Reynolds stress term, namely the shear stress, the equations governing these linearized perturbations become

$$U_0 \frac{\partial u}{\partial x} + \frac{\mathrm{d}U_0}{\mathrm{d}z} w + \frac{\partial p}{\partial x} = \frac{\partial \tau}{\partial z} - f,$$

$$U_0 \frac{\partial w}{\partial x} + \frac{\partial p}{\partial z} = 0,$$

$$\frac{\partial u}{\partial x} + \frac{\partial w}{\partial z} = 0. \tag{4.1}$$

On elimination of the pressure, these equations combine to yield

$$U_0 \left(\frac{\partial^2 w}{\partial z^2} + \frac{\partial^2 w}{\partial x^2} \right) - U_0'' w = \frac{\partial f}{\partial z} - \frac{\partial^2 \tau}{\partial z^2}. \tag{4.2}$$

The boundary conditions are first that the perturbations decay far from the canopy and secondly no-slip at the surface. This is justified even within the canopy because the spatially averaged wind, namely $U_0 + u$, is defined to be the wind averaged within the fluid volume only, where the no-slip condition is satisfied.

The mixing-length model is also linearized to yield a relationship between the perturbation stress and the perturbation velocity gradient:

$$\tau = 2u_* l_m \partial u / \partial z. \tag{4.3}$$

As explained in §2.2, the mixing length is parameterized either as the standard mixing length (2.6) or the displaced mixing length (2.17).

The range of validity of the linearized equation (4.2) is established by estimating the magnitude of the linear perturbations compared to the magnitude of the upstream flow. The characteristic velocity scale in the incident flow is U_h, defined at the height of the canopy, so that

$$U_h = U_0(h) = (u_*/\kappa) \ln(h/z_0). \tag{4.4}$$

The forcing for the perturbations is the drag force, and hence the magnitude of the maximum streamwise velocity perturbation induced over the whole length of the canopy can be estimated by balancing the acceleration term over the length of the canopy, $U_0 \partial u / \partial x \sim U_h u / L$, with the drag term, $f \sim U_h^2 / L_c$, which yields the

following linear estimate for the velocity perturbation

$$u \sim U_h L/L_c. \tag{4.5}$$

Hence, for a *weak canopy*, with $L/L_c \ll 1$, the perturbation velocities are small, $u \ll U_h$, and the linearized equation (4.2) is appropriate.

Secondly, as is usual in these perturbed boundary-layer problems (e.g. Townsend 1976, p. 307; Belcher & Hunt 1998), the stress gradient term is smaller than the acceleration term over significant regions of the flow. This can be shown by examining the ratio of these two terms over vertical and horizontal length scales L. In the particular case when the mixing-length model is used:

$$\frac{\partial \tau/\partial z}{U_0 \partial u/\partial x} = \frac{(\partial/\partial z)(2u_* l_m \partial u/\partial z)}{U_0 \partial u/\partial x} \sim \frac{u_*/l_m}{U_h/L} \ll 1. \tag{4.6}$$

Asymptotic methods can then be used to obtain solutions to (4.2) in the limit that u_*/U_h is small. Now the definition of U_h shows that the analysis requires

$$\frac{u_*}{U_h} = \frac{1}{(1/\kappa)\ln(h/z_0)} \ll 1, \tag{4.7}$$

which is usually satisfied because the upwind roughness length is much smaller than the height of the canopy.

It is convenient to treat the resulting mathematical problem in Fourier space, defined, for example, for the streamwise velocity perturbation, $\tilde{u}(k, z)$, by

$$u(x, z) = \frac{1}{2\pi} \int_{-\infty}^{\infty} \tilde{u}(k, z) e^{ikx} \, dk. \tag{4.8}$$

Application of this Fourier transform to the equation governing the vertical velocity, (4.2), yields

$$U_0 \left(\frac{d^2 \tilde{w}}{dz^2} - k^2 \tilde{w} \right) - U_0'' \tilde{w} = \frac{d\tilde{f}}{dz} - k^2 \tilde{\tau} - \frac{d^2 \tilde{\tau}}{dz^2}. \tag{4.9}$$

With the mixing-length model for the turbulent shear stress, (4.9) becomes a fourth-order ordinary differential equation. There are four boundary conditions: u, w are zero at the surface and u, w decay to zero far above the canopy. Solutions to this equation correspond to the vertical velocity induced by a force that varies sinusoidally in the x-direction about a zero mean. In the linear model, the force variation in the vertical and horizontal directions have to be specified. Solutions for flow through a canopy that varies arbitrarily in the streamwise direction are obtained by numerical inversion of the Fourier transforms.

4.2. *The inviscid approximation to the impact and adjustment regions*

As shown above, the shear stress is much smaller than the inertial terms over much of the flow. A first approximation to the flow is then calculated by solving (4.9), neglecting the two terms involving the shear stress. A further approximation is to neglect the curvature in the incident wind profile, $U_0''/k^2 U_0$, which is small away from the surface in a logarithmic incident profile. Solutions based on these approximations are described in §4.2.1 and §4.2.2.

These inviscid solutions provide useful quantitative estimates in region (i) where the flow impacts onto the canopy and demonstrates how the mean velocity field (even without the shear stress) adjusts smoothly from upwind to its form within and above the canopy. In addition, as will be shown in §4.2.3, in the impact region, a

generalization of the inviscid theory can provide insights into the effects of the finite volumes of the canopy elements.

4.2.1. *General solution in the inviscid approximation*

Equation (4.9) is approximated as described above, when it reduces to (the Fourier transform of) Poisson's equation. The resulting equation can be solved using Green's function methods to give

$$\tilde{w} = Ce^{-kz} + De^{kz} + \int_{z_0}^{z} \tilde{f}(k, z') \frac{\cosh(z - z')}{U_0(z')} \, dz', \tag{4.10}$$

where C and D are coefficients determined by boundary conditions (the notation is chosen to be consistent with Jerram 1995, chapter 3). The solutions for the streamwise velocity and pressure perturbations are then found from continuity and the streamwise momentum equation, respectively, to yield

$$\tilde{u} = -iCe^{-kz} + iDe^{kz} - \frac{\tilde{f}}{ikU_0(z)} + \int_{z_0}^{z} \tilde{f}(k, z') \frac{\sinh(z - z')}{U_0(z')} \, dz' \tag{4.11}$$

$$\tilde{p} = iU_0(z) \left\{ Ce^{-kz} - De^{kz} - \int_{z_0}^{z} \tilde{f}(k, z') \frac{\sinh(z - z')}{U_0(z')} \, dz' \right\}. \tag{4.12}$$

The coefficient D is determined by the condition that the perturbations decay far from the canopy, which implies that

$$D + \frac{1}{2} \int_{z_0}^{\infty} \tilde{f}(k, z') \frac{e^{-kz'}}{U_0(z')} \, dz' = 0. \tag{4.13}$$

The second coefficient, C, is determined with the boundary condition that the vertical velocity is zero at the surface, $z = z_0$, which yields

$$C + D = 0. \tag{4.14}$$

Higher-order corrections to this leading-order solution that account for small, but finite, curvature in the upwind velocity profile have been derived (Jerram 1995, §3.5.7).

4.2.2. *Inviscid solution for a rectangular canopy*

For a constant drag in a rectangular region, lying between $x = -L/2$ and $L/2$, namely

$$f = \frac{U_h^2}{L_c} \left\{ \mathcal{H}(x + L/2) - \mathcal{H}(x - L/2) \right\} \left\{ 1 - \mathcal{H}(z - h_e) \right\}, \tag{4.15}$$

where $\mathcal{H}$ is the Heaviside step function, the solutions can be evaluated explicitly in physical space to yield

$$u(x, z) = \frac{U_h L/L_c}{4\pi} \left[h_1(\hat{x} - \tfrac{1}{2}, \hat{z} - \hat{h}_e) - h_1(\hat{x} + \tfrac{1}{2}, \hat{z} - \hat{h}_e) \right.$$
$$\left. - h_1(\hat{x} - \tfrac{1}{2}, \hat{z} + \hat{h}_e) + h_1(\hat{x} + \tfrac{1}{2}, \hat{z} + \hat{h}_e) - 4\pi(1 - \mathcal{H}(z - h_e)) \right], \tag{4.16}$$

$$w(x, z) = -\frac{U_h L/L_c}{4\pi} \left[h_2(\hat{x} - \tfrac{1}{2}, \hat{z} - \hat{h}_e) - h_2(\hat{x} + \tfrac{1}{2}, \hat{z} - \hat{h}_e) \right.$$
$$\left. - h_2(\hat{x} - \tfrac{1}{2}, \hat{z} + \hat{h}_e) + h_2(\hat{x} + \tfrac{1}{2}, \hat{z} + \hat{h}_e) \right]. \tag{4.17}$$
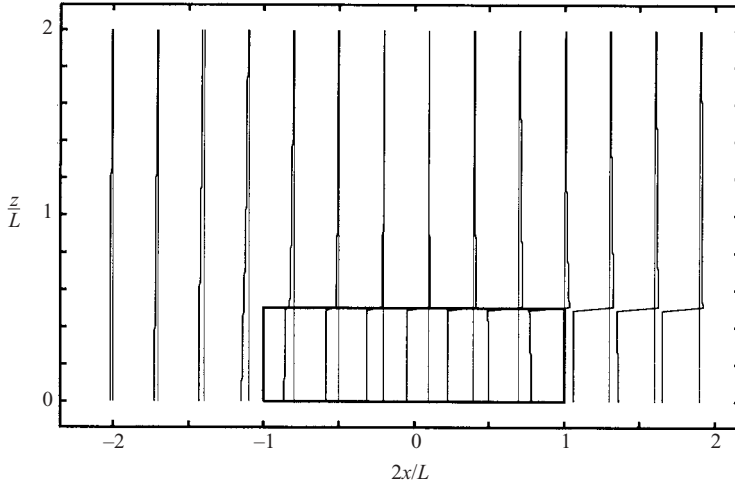
FIGURE 4. Inviscid perturbations, u/U_h, to a uniform incident flow, U_h, at a succession of downstream locations through a canopy with constant drag force, $f = 0.45U_h^2/L$ and $h/L = 0.5$ (so that $L/L_c \approx 0.5$). Note the non-zero perturbation at the surface and the discontinuity in u at the top of the canopy. At the end of the canopy and in the wake $u/U_h = -0.83$.

Here, $\hat{x} = x/L$, $\hat{z} = z/L$, $\hat{h}_e = h_e/L$ and

$$h_1(\xi, \zeta) = \zeta \ln\left(\xi^2 + \zeta^2\right) - 2\xi \tan^{-1}\left(\xi/\zeta\right), \tag{4.18}$$

$$h_2(\xi, \zeta) = -\xi \ln\left(\xi^2 + \zeta^2\right) - 2\zeta \tan^{-1}\left(\xi/\zeta\right), \tag{4.19}$$

where the inverse tangents are defined to lie within $-\pi/2$ and $\pi/2$, so that care is needed in evaluating the solutions across the branch cuts around the boundary of the canopy.

We have argued that over significant regions of the flow, the solution is dominated by inviscid irrotational processes. Hence, figure 4 shows profiles of the streamwise velocity as a uniform flow, U_h, impinges upon a rectangular canopy with a constant resistive force, $f = 0.45U_h^2/L$, calculated using the inviscid solution (4.16). The solution shows clearly how the wind speed decelerates in the impact region, and within the canopy, with an increasing velocity deficit through the canopy. Above the canopy, the wind speed is decelerated and then beyond halfway, it is accelerated: the canopy acts as a source above the canopy. In the inviscid approximation, the drag-induced velocity deficit remains constant in the wake downwind of the canopy and does not decay.

The solution (4.16) and the profiles in figure 4 show that upwind of the canopy, within the impact region, the flow decelerates over a length of order L. Just at the upwind edge of the canopy at the surface the inviscid solution (4.16) gives

$$u(-L/2, z_0) = U_h \left[-\frac{1}{2\pi} \frac{h_e}{L_c} \ln\left(\frac{h_e^2 + L^2}{h_e^2}\right) + \frac{L}{4\pi L_c} \left\{ 4\tan^{-1}\left(\frac{L}{2h_e}\right) - 2\pi \right\} \right]$$

$$\approx -\frac{U_h}{2\pi} \frac{h_e}{L_c} \ln\left(1 + \frac{L^2}{h_e^2}\right), \tag{4.20}$$

when the canopy is long, $L \gg h_e$, so that $4\tan^{-1}(L/2h_e) \to 2\pi$.

This result is from the linear solution, which requires $L/L_c \ll 1$. The deceleration of the flow within the canopy leads to a perturbation mass flux outwards. When L

is comparable to or greater than L_c, only in the adjustment region is there a mass flux out of the canopy. Downwind, there is a slowly varying weak flow within the canopy (if $h_e \geqslant l_s$). Hence, an estimate for the deceleration upwind of the canopy for more typical canopies that have $L \geqslant L_c$ that accounts for this nonlinear process (but ignores others) is obtained by replacing L with L_c in (4.20) to yield

$$u(-L/2, z_0) = -\frac{U_h}{2\pi} \frac{h_e}{L_c} \ln\left(1 + \frac{L_c^2}{h_e^2}\right). \tag{4.21}$$

Later this expression will be compared to measurements.

4.2.3. *Effects of canopy elements of finite volume in the impact region*

The analysis developed above shows how the aerodynamic resistance of the roughness elements within the canopy decelerates the flow over a distance of order L upwind of the canopy and leads to a velocity perturbation (4.21) just upwind of the canopy. Now, when the canopy elements have a finite volume, the streamlines are also displaced over and around the canopy elements. This displacement also leads to a deceleration of the (spatially averaged) mean flow, U.

The magnitude of this deceleration can be estimated by calculating the inviscid irrotational perturbations to a uniform upwind flow, of magnitude U_h, caused by a set of obstacles mounted on a surface. The resulting potential flow induced by the bodies is then averaged over a horizontal area $(g_e + b_e) \times (g_e + b_e)$ to estimate the deceleration of the mean flow induced by an canopy of elements of finite volume.

If the canopy elements are either cuboidal, so that $b_e \sim w_e \sim h_e$, or tall thin cylinders mounted vertically, so that $b_e \ll h_e$ and the flow is predominantly around the obstacles, then the perturbation velocity near the surface a distance $(g_e + b_e)$ upwind of the canopy is of order

$$\frac{u}{U_h} \sim -\frac{b_e^2}{(g_e + b_e)^2}, \tag{4.22}$$

and the deceleration decays algebraically upwind of the canopy on the length scale $g_e + b_e$.

We shall see evidence in the comparisons with measurements described in §5 of these decelerations associated with the finite volumes of the canopy elements.

4.3. *Effects of the turbulent stress gradients*

As the profiles in figure 4 show, the inviscid solution is incorrect both at the surface, because it does not satisfy the no-slip condition, and at the top of the canopy, where discontinuity in the force distribution yields large vertical gradients in the streamwise velocity perturbations. Within thin layers, referred to here as *inner layers*, centred at these two levels, the turbulent shear stress gradient become comparable to the inertial terms, and a new analysis is required.

Following analyses of flow over hills (Jackson & Hunt 1975; Belcher & Hunt 1998; Hunt, Leibovich & Richards 1988) and flow over roughness changes (Belcher *et al.* 1990), the stress gradient and advection terms, namely the first and sixth terms in (4.9), are comparable in the inner layers, which on using the linearized version of the mixing-length model (4.3) yields

$$-\frac{d^2}{dz^2}\left(\frac{2\kappa u_* z}{ik} \frac{d^2 \tilde{w}}{dz^2}\right) \sim U_0(z) \frac{d^2 \tilde{w}}{dz^2}. \tag{4.23}$$

If the inner layer is centred at height h_i, (4.23) yields an estimate for the thickness, l_i, of the inner layer, namely

$$k^2 l_i^2 \sim k h_i \frac{u_*}{U_0(h_i)}. \tag{4.24}$$

The inner layer at the ground within the canopy, where the wind velocity decreases to zero to satisfy the no-slip condition, then has $h_i = l_i$, so that $k l_i \sim u_*/U_0(l_i)$, which is small. The inner layer at the top of the canopy has $h_i = h_e$, so that $k^2 l_i^2 \sim k h_e u_*/U_h$, which is also small. Hence, the inner layers are thin. This means first that, within the inner layers, streamwise gradients, $\partial/\partial x$, can be neglected compared with vertical gradients, $\partial/\partial z$. Secondly, the shear in the incident wind profile is small in the thin inner layers and so the value of the incident wind profile can be approximated by its value at the layer height, i.e. $U_0(z) \approx U_0(h_i)$. Thirdly, the curvature term in (4.9) is smaller within the inner layer than the advection term because their ratio is small:

$$\frac{U_0'' \tilde{w}}{U_0 \mathrm{d}^2 \tilde{w}/\mathrm{d}z^2} \sim \frac{u_*}{U_0(h_i)} \ll 1. \tag{4.25}$$

Hence, to leading order, the flow in the inner layers is governed by

$$-\frac{\mathrm{d}}{\mathrm{d}z} \left\{ \frac{\mathrm{d}}{\mathrm{d}z} \left(\frac{2\kappa u_* l_m}{\mathrm{i}k} \frac{\mathrm{d}^2 \tilde{w}}{\mathrm{d}z^2} \right) - U_0(h_i) \frac{\mathrm{d}\tilde{w}}{\mathrm{d}z} \right\} = \frac{\mathrm{d}\tilde{f}}{\mathrm{d}z}. \tag{4.26}$$

This equation can be integrated once with respect to z. The integration constant is $\mathrm{i}k \tilde{p}(h_i)$, the perturbation pressure, which is approximately constant with height over the thin inner layer. On using continuity, $\mathrm{d}\tilde{w}/\mathrm{d}z = -\mathrm{i}k\tilde{u}$, the leading-order equation governing dynamics of inner layers, becomes

$$\frac{\mathrm{d}}{\mathrm{d}z} \left(2\kappa u_* l_m \frac{\mathrm{d}\tilde{u}}{\mathrm{d}z} \right) - \mathrm{i}k U_0(h_i)\tilde{u} = \tilde{f} + \mathrm{i}k \tilde{p}(h_i). \tag{4.27}$$

Hence, any imbalance between streamwise advection, canopy drag and the pressure perturbation driven by the inertial forces is balanced by vertical transport of momentum by the stress gradient. The solution to (4.27) depends on the model used for the mixing length. Explicit solutions for the standard mixing length and the displaced mixing length are developed next.

4.3.1. *Solution with the standard mixing-length model*

As described above, for a uniform canopy of depth h_e there are inner layers around the top of the canopy, $z = h_e$, and at the surface $z = 0$. Focus initially on the inner layer at the surface.

The most general solution to (4.27) is found using Green's function methods, and with the standard mixing-length model, $l_m = \kappa z$, Jerram (1995, § §3.5, 3.6) shows that

$$\tilde{u} = A J_0(Z) + B K_0(-\mathrm{i}Z) - \frac{\tilde{p}}{U_0(h_i)}$$

$$- \frac{1}{\mathrm{i}k U_0(h_i)} \int_{Z_0}^{Z} Z' \tilde{f}(k, z') \{ J_0(Z) K_0(-\mathrm{i}Z') - J_0(Z') K_0(-\mathrm{i}Z) \} \, \mathrm{d}Z', \tag{4.28}$$

where $J_0(Z)$ and $K_0(-\mathrm{i}Z)$ are Bessel functions (Abramowitz & Stegun 1972, chapter 9). The first, $J_0(Z)$, increases exponentially for large Z and the second, $K_0(-\mathrm{i}Z)$, decays exponentially for large Z. The Bessel functions are functions of a rescaled height

variable defined by

$$Z = \exp(3i\pi/4) \left(\frac{U_0(h_i)}{\kappa u_*} kz \right)^{1/2}. \tag{4.29}$$

Note how $\tilde{f}$ in (4.28) remains a function of the unscaled height z.

The coefficients A and B in (4.28) are determined by the boundary conditions. Far above the inner layer, the solution must remain finite, so that the coefficient of $J_0(Z)$ must be zero at large Z, which yields

$$A - \frac{1}{ikU_0(h_i)} \int_{Z_0}^{\infty} Z' f(k, z') K_0(-iZ') \, dZ' = 0. \tag{4.30}$$

Towards the surface, $J_0(Z)$ tends to zero, whereas $K_0(-iZ)$ diverges logarithmically. The logarithmic divergence is avoided, and the no-slip condition is satisfied for the inner layer at the surface, if B satisfies

$$A J_0(Z_0) + B K_0(-iZ_0) - \frac{\tilde{p}(h_i)}{U_0(h_i)} = 0, \tag{4.31}$$

where Z_0 is the value of Z at $z = z_0$.

The final condition required to determine the final coefficient in (4.10) and (4.28), namely $\tilde{p}(h_i)$, is obtained by calculating the pressure in the inner layer, which is determined from the solution for the pressure in the inviscid layer (4.12) taken in the limit of small z. This procedure yields

$$\tilde{p}(h_i) = iU_0(h_i)(C - D), \tag{4.32}$$

where C is given by (4.14) and D is given by (4.13).

The inner layer around the top of the canopy has formally the same solution, namely (4.28), but with $d_i = h_e$. Both inner layers are then neatly accounted for if $U_0(h_i)$ is replaced by $U_0(z)$ throughout the solutions to the inner layer obtained above.

Hence, all the coefficients are determined: (4.13) determines D, (4.14) determines C, (4.30) determines A, (4.31) determines B, and (4.32) determines $\tilde{p}(h_i)$. The solution with the standard mixing-length model is then complete. Jerram (1995, § 3.5.8) shows that the small downstream thickening of the inner layer leads to a small vertical velocity, so that when higher-order linear effects are calculated, $C + D$ in (4.14) has a very small contribution, of order u_*^2/U_h^2.

4.3.2. *Solution with the displaced mixing-length model*

With the displaced mixing-length model, in the flow through the bulk of the canopy, $z < z_c$, the mixing length is constant and so, in the linearized framework, the perturbation flow is governed by a constant viscosity, namely $\nu_t = 2\kappa u_* l_m$. Solutions for the perturbations to the flow within the canopy can then be calculated from (4.2) with no further approximation.

Hence, following Jerram (1995, § 3.8.5), the solution to (4.2) in $z < z_c$ is calculated using Green's function methods, and is found to be

$$\begin{aligned}
\tilde{w} = {} & E[\sinh\{\alpha(z - z_0)\} - (\alpha/\beta)\sinh\{\beta(z - z_0)\}] \\
& + F[\cosh\{\alpha(z - z_0)\} - \cosh\{\beta(z - z_0)\}] \\
& - \frac{ik}{2\kappa u_* l_m} \int_{z_0}^{z} \frac{\partial f}{\partial z}(k, z') \left[\frac{\sinh\{\alpha(z - z')\}}{\alpha(\alpha^2 - \beta^2)} - \frac{\sinh\{\beta(z - z')\}}{\beta(\alpha^2 - \beta^2)} \right] dz'. \tag{4.33}
\end{aligned}$$

Here $\alpha^2 = k^2 + ikU_h/\nu_t$ and $\beta = |k|$, and E and F are coefficients that are determined by boundary conditions. The streamwise velocity perturbation is obtained from continuity and the pressure perturbation from the streamwise momentum equation, thus

$$\tilde{u} = -\frac{1}{ik}\frac{\partial \tilde{w}}{\partial z}, \tag{4.34}$$

$$\tilde{p} = -\frac{2\kappa u_* l_m}{k^2}\left(\frac{\partial^3}{\partial z^3} - k^2\frac{\partial}{\partial z}\right)\tilde{w} + \frac{U_h}{ik}\frac{\partial \tilde{w}}{\partial z} + \frac{\tilde{f}}{ik}, \tag{4.35}$$

$$\tilde{\tau} = -\frac{2\kappa u_* l_m}{ik}\left(\frac{\partial^2}{\partial z^2} - k^2\right)\tilde{w}. \tag{4.36}$$

Above z_c, the mixing length increases with height, $l_m = \kappa(z - d)$, where d is the displacement height. Hence, the solution here has inner-layer dynamics, and so the approximate solution is formally the same as (4.28), but with the height z replaced by the displaced height $z - d$. Hence, the solution is (4.28) with

$$Z = \exp{(3i\pi/4)}\left(\frac{U_0(h_i)}{\kappa u_*}k(z - d)\right)^{1/2}. \tag{4.37}$$

The two coefficients, A and B, in this solution are determined by matching with the inviscid layer that applies above the inner layer at the top of the canopy, and proceeds exactly as in §4.3.1. The inviscid component of the solution is also written in terms of $z - d$, namely

$$\tilde{w} = Ce^{-k(z-d)} + De^{k(z-d)} + \int_{z_0}^{z-d}\tilde{f}(k, z')\frac{\cosh{(z - z')}}{U_0(z')}\,dz'. \tag{4.38}$$

The inner-layer solution must also match with the solution in the canopy mixing layer, where the velocity perturbations are $\tilde{u}_c$ and $\tilde{w}_c$. Hence, the solutions above the canopy mixing layer are the same as with the standard mixing-length model but with an effective origin at the displacement height $z = d$, and with additional velocity perturbations $\tilde{u}_c$ and $\tilde{w}_c$. The remaining constants E and F, which can be related to $\tilde{u}_c$ and $\tilde{w}_c$, are found by ensuring that $\tilde{p}$ and $\tilde{\tau}$ are continuous at the top of the layer of constant mixing length. In the solutions calculated here, these coefficients were calculated numerically: the procedure is straightforward but lengthy, for details, see Jerram (1995, §3.8.7).

4.4. *Numerical implementation*

The solutions derived above are for the Fourier transforms of the perturbations to the flow induced by a weak force distribution, with Fourier transform $\tilde{f}(k, z)$. The procedure for obtaining solutions for a realistic force distribution that varies in the streamwise direction, $f(x, z)$ is as follows. The Fourier transform is taken numerically of the force distribution, $f(x, z)$, to yield $\tilde{f}(k, z)$. The solutions obtained above, which depend upon $\tilde{f}(k, z)$, are then evaluated numerically for each k. These solutions for the Fourier transforms of the perturbation flow, e.g. $\tilde{u}(k, z)$, are then inverted numerically using a fast Fourier transform to obtain the perturbations in physical space according to (4.8).

In fact, the solutions contain a logarithmic singularity at zero wavenumber. This singularity must be treated correctly because most force distributions of interest have non-zero power at $k = 0$, and hence this part of the inverse Fourier transforms contributes to the solutions. (The force distribution has zero power at $k = 0$ only if the
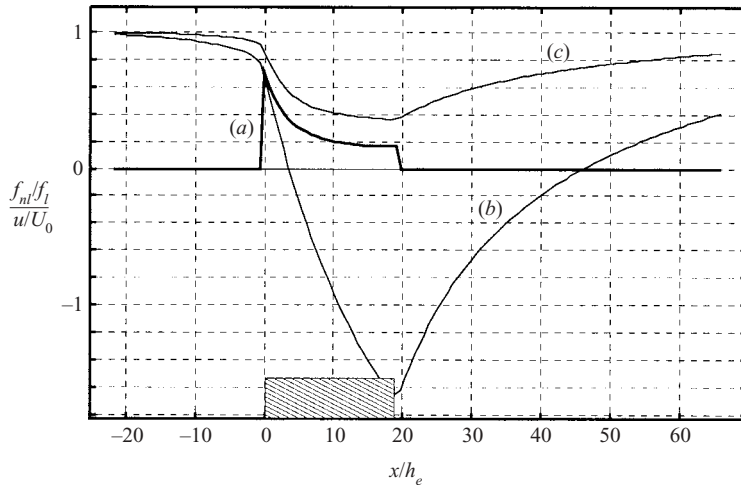
FIGURE 5. The effect of iterating the force. (*a*) The ratio of the force after iteration to before iteration, integrated over the height of the canopy. (*b, c*) Streamwise velocity at half the canopy height, before and after iteration, normalised on undisturbed wind speed at half the canopy height. The horizontal axis is streamwise distance from leading edge normalised on the canopy height. The position of the canopy is shown as hatched.

force distribution is such that $\int_{-\infty}^{\infty} f(x, z)\, \mathrm{d}x = 0$, which is not typical.) The singularity is treated by integrating the small-wavenumber range separately by changing the integration variable to $\ln k$. See Jerram (1995, §4.3) for details.

Finally, as explained in §2.1, the force distribution is written for practical applications as $f = U^2/L_c$. In a strictly linear analysis, the forcing then becomes $f = U_0^2/L_c$ with $U_0(z)$ the upstream undisturbed velocity profile. With this strictly linear model, the flow can never adjust to a balance between the stress gradient and the canopy drag, because the canopy drag does not adjust. Hence, such a strictly linear model can only describe the adjustment region described in §3.

The strictly linear model can be improved upon significantly by accounting for the nonlinear drag, yielding a quasi-linear model. The procedure is to iterate numerically the linearized solutions obtained analytically as follows. On the first iteration, f is specified using the undisturbed velocity profile $U_0(z)$. The streamwise velocity perturbations are then calculated. A new force distribution is then constructed using the computed streamwise velocity $U_0 + u$. This force distribution is then used in the analytical solutions to compute the next iteration for the streamwise velocity perturbation. The process is repeated until the solution changes by less than a specified tolerance. In the examples considered below, the solutions converged in three or four iterations.

The effect of the nonlinear correction renders the model a useful predictive tool, as shown below. Figure 5 shows results from a simulation with a rectangular region of drag (using the parameters of the experiment of Davidson *et al.* 1995*a*, which are described below). It shows the ratio of the drag f calculated with and without iteration and the streamwise velocity at half the canopy height with and without iteration. This figure demonstrates the importance of the iteration: without iteration the streamwise velocity perturbation continues to decrease through the canopy, whereas with iteration, it comes more nearly into equilibrium.

5. Comparison of model results with previous studies

The objective of the present study has been to elucidate scalings for adjustment to a canopy and also to develop a quantitative model. Therefore, any parameters of the model are estimated on the basis of physical arguments, the flow that result from the estimated parameter set is then calculated, and the results compared with simulations or experiment.

Each of the comparisons below shows a different aspect of the fluid dynamics: §5.1 shows how the quasilinear model compares with a numerical model with all nonlinear terms; §5.2 shows adjustment to a fine-scale (forest) canopy; §5.3 shows recovery and then impact in a fine-scale canopy; and §5.4 shows adjustment to a canopy of large roughness elements, when we suggest the finite-volume process becomes important.

5.1. *Comparison with the numerical model of Svensson & Häggkvist*

Svensson & Häggkvist (1990) performed a numerical simulation of two-dimensional mean flow through a distributed resistance in a rectangular region with $h_e = 2.5\,\mathrm{m}$ and $L = 250\,\mathrm{m}$. The distributed resistance was calculated from $f = \bar{c}_d a |U|U/2$, with a drag coefficient $\bar{c}_d = 0.3$, and a 'plant area density', $a = 2.1\,\mathrm{m}^{-1}$, which yields $L_c = (\bar{c}_d a/2)^{-1} = 3.2\,\mathrm{m}$, so that $h_e/L_c = 0.8$. This is a shallow canopy.

The turbulent stress was modelled by Svensson & Häggkvist using a modified form of the $k-\varepsilon$ closure model. Small-scale wake turbulence generated by the canopy increases small-scale dissipation (Kaimal & Finnigan 1995, chapter 3), which Svensson & Häggkvist represent by introducing new source terms based on $\bar{c}_d$, a and U into the equations for turbulent kinetic energy and turbulent dissipation. Svensson & Häggkvist adjusted the coefficients multiplying these new source terms to give good agreement with canopy velocity profiles measured in the experiment of Raupach *et al.* (1986) far downstream of the adjustment region.

The incident velocity profile used by Svensson & Häggkvist was

$$U(z) = 10 \left(\frac{z}{110\,\mathrm{m}} \right)^{1/7} \mathrm{m\,s^{-1}}. \tag{5.1}$$

For comparison with the present model, a logarithmic profile was fitted to (5.1) by matching velocities at $z = h_e$ and $z = h_e/2$. This gives $z_0 = 1.604\,\mathrm{mm}$ and $u_* = 0.3248\,\mathrm{m\,s^{-1}}$. The fitted logarithmic profile then differs from (5.1) by less than 3% over the height range $0.4\,\mathrm{m} < z < 11\,\mathrm{m}$, which includes the part of the canopy where the distributed force and velocity perturbations are most significant.

The present model, with the simple mixing length, was used to compute the flow through a rectangular canopy. Results in the exit region of the canopy calculated from the present model are compared with Svensson & Häggkvist's results in figure 6. The points are simulation data measured from Svensson & Häggkvist's figure 4a. The curves are from the present model. The agreement is satisfactory, giving confidence that the quasi-linear model developed here is useful in representing the nonlinear adjustment computed by Svensson & Häggkvist's fully-nonlinear model.

5.2. *Flow through a model plant canopy*

Meroney (1968) measured the turbulent flow in and above a model forest consisting of trees made from 'plastic simulated-evergreen boughs'. His forest canopy was $0.18\,\mathrm{m}$ high and $11\,\mathrm{m}$ long with tree density one per $36\,\mathrm{cm}^2$. Meroney gives the tree drag coefficient as $\bar{c}_d = 0.72$ and his description of the model tree shape gives a frontal area of $71.5\,\mathrm{cm}^2$. Hence, the projected frontal area of the tree crown is $a_f = 11.0\,\mathrm{m}^{-1}$. The leaf area index a may be greater or less than a_f depending upon leaf distribution
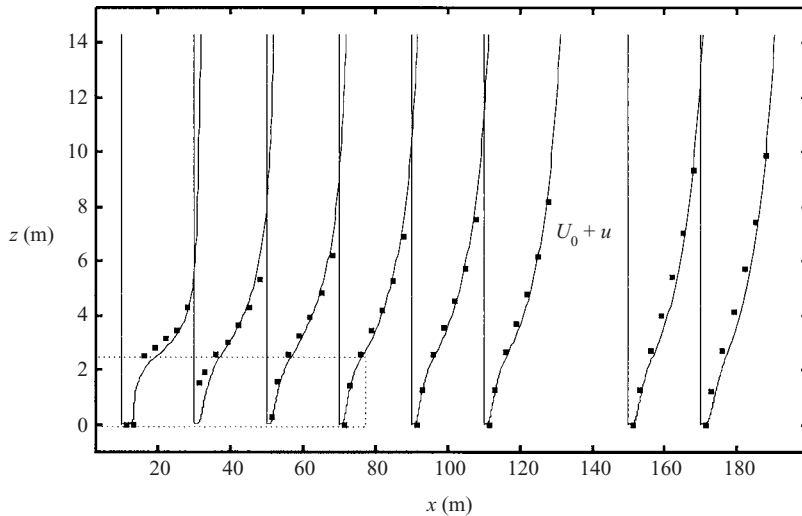
FIGURE 6. Profiles of streamwise velocity in the exit region of a canopy, whose position is shown as hatched. Points: numerical simulation of Svensson & Häggkvist (1990). Curves: current theory with the simple mixing-length model.

and orientation within the crown. The occupied volume fraction β is half the volume porosity of the tree crown. In the absence of more precise information, we estimate $a/(1 - \beta) = a_f$. With this data, and assuming that the drag is uniformly distributed with height, the canopy-drag length scale is estimated from (2.4) to be $L_c = 0.13$ m. Hence, $h_e/L_c = 1.4$ and this is a deep canopy, typical of forests. Jerram (1995, §4.7) also shows calculations with a higher drag in the tree crown than in the trunk space. The results are almost indistinguishable from the results with the uniform drag and are not further discussed here.

Meroney did not specify an incident velocity profile. It is estimated here by fitting a logarithmic profile to his measured profile at $x = -1$ m. This gives $z_0 = 1.77$ mm and $u_* = 0.391 \, \text{m s}^{-1}$. The present model was also used to compute the flow using the displaced mixing-length model. The parameters for the displaced mixing-length model are estimated to be $l_c/h_e = 0.2$, $d/h_e = 0.7$ and $z_c/h = 0.75$. The low value of l_c/h_e reflects the small horizontal length scale of the model forest elements (which were less than about 5 cm) in comparison with canopy height. The value of d/h_e is an estimate following Thom (1971) and Jackson (1981) of the level of mean momentum absorption, and is typical of the ratios observed. These values of z_c and d imply that the effective roughness length of the canopy is $z_0^{eff} = 0.05h_e \approx 1$ cm.

The comparison between present theory and experiment is shown in figure 7 (simple mixing-length model) and figure 8 (displaced mixing-length model). In general, the agreement is good, and more so for the downstream half of the canopy than for the upstream half. Note also that the deceleration of the flow ahead of the canopy obtained from (4.21) is $u/U_0 = -0.24$, which is about a quarter of the maximum velocity deficit in the canopy, in agreement with the computations and the measurements.

The results for the overall form of the flow obtained from the simple and displaced mixing-length model calculations are similar. In particular, the growth of the maximum velocity defect is similar in both cases. This similarity occurs because the maximum velocity deficit is controlled largely by the inviscid dynamics, as explained in §3.
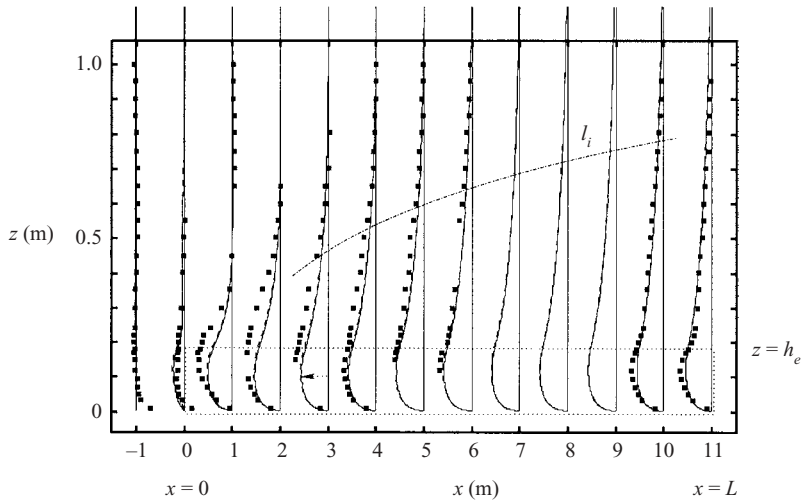
FIGURE 7. Profiles of perturbations to the streamwise velocity through Meroney's (1968) wind tunnel model of a forest canopy. Points: values measured by Meroney (1968). Solid lines: current theory using the simple mixing-length model. Dotted line: boundary of the canopy; dot-dash line: sketch of the development of the internal boundary layer that develops over the canopy interior.
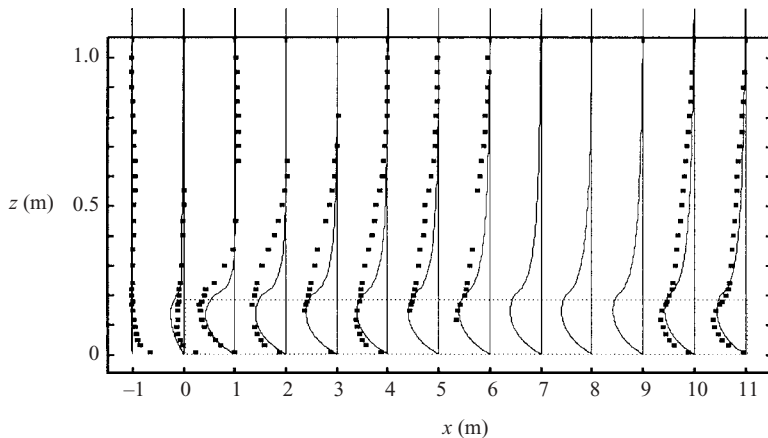

FIGURE 8. Comparison of Meroney's (1968) wind tunnel model of a forest canopy with the present model using the displaced mixing-length model with $l_c/h_e = 0.2$, $d/h_e = 0.7$ and $z_c/h_e = 0.75$. Perturbation streamwise velocity is plotted against height at a series of downstream locations. Points: experimental data. Solid lines: current theory.

5.3. *The effect of a clearing in mid-forest*

Next the model is applied to a mean wind acceleration in a clearing in mid-forest investigated by Stacey *et al.* (1994) using model trees in a wind-tunnel experiment. Stacey *et al.* modelled a spruce forest with average height $h_e = 15$ m, with far upstream roughness height 0.1 m, across which a clearing had been cut 6.7 tree heights (100.5 m) wide. They assumed that the full-scale drag of an isolated tree D (in Newtons) agreed with an empirical formula due to Mayhead, Gardiner & Durrant
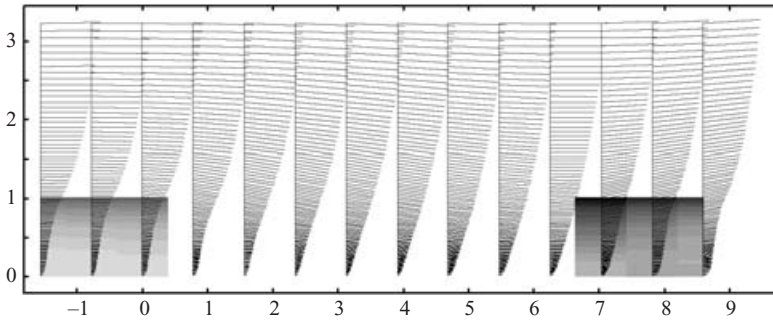
FIGURE 9. Velocity vectors in a clearing in mid-forest. Coordinates are non-dimensionalized on the forest canopy height $h = 15$ m. Grey scale within the canopy indicates the strength of the local force on the canopy: the largest force acts at the leading edge of the canopy following the clearing.

(1975), namely,

$$D = 0.4352U^2 m^{0.667} \exp(-0.0009779U^2), \tag{5.2}$$

where m is the tree's live branch mass in kg and U is the nominal incident wind speed in m s^{-1}. In the conditions being modelled, the live branch mass was $m = 49.5$ kg and the nominal wind speed 30 m s^{-1}, hence the drag force on an isolated full-scale tree was 2193 N. The lateral and streamwise tree spacings were 1.73 m, so the canopy volume per tree was 44.9 m^3. Therefore, the canopy adjustment length scale may be estimated as

$$\frac{1}{L_c} = \frac{2193 \, \text{N}}{\frac{1}{2}\rho \times 30^2 \, \text{m}^2 \, \text{s}^{-2} \times 44.9 \, \text{m}^3} \approx 0.11 \, \text{m}^{-1}, \tag{5.3}$$

so that $L_c = 9$ m and this is again a deep canopy with $h_e/L_c = 1.7$.

The flow field shown in figure 9 is calculated using two regions of distributed force. Both are 15 m high and have $L_c = 9$ m. One extends from $x = -500$ m to $x = 0$ and is intended to set up an equilibrium canopy flow. The other extends from $x = 100.5$ m to $x = 300$ m. The clearing lies between the two regions. The experimentally measured flow field is shown in Stacey *et al.*'s (1994) figure 13. Detailed numerical comparison is not attempted here; there is qualitative agreement between the experimental data presented in Stacey *et al.* and the present model. The most notable feature is the vertical velocity variation within the clearing. The wind turns downwards to fill out the clearing immediately after its upstream edge and only turns upwards again after the trailing edge when the blocking effect of the downstream resistance has become dominant.

The shaded contours over the canopy regions in figure 9 represent the strength of the local distributed force. The darker contours at the downstream edge of the clearing indicate that the force acting is stronger here than in the equilibrium flow at the left-hand edge of the figure. Hence, a clearing in a forest increases the risk of local wind damage, as observed by Stacey *et al.*

5.4. *Deceleration of the mean wind through a building canopy*

Davidson *et al.* (1995a,b) conducted two experiments on a staggered array of obstacles, arranged as shown in figure 10, more typical of an urban canopy with $h_e/L_c < 1$. One was a full-scale field experiment with obstacle dimensions (refer to figure 10) $w_e \times b_e \times h_e = 2.2$ m $\times$ 2.45 m $\times$ 2.3 m, with $L = 44.1$ m, the other a wind-tunnel experiment with $w_e = b_e = h_e = 0.12$ m, with $L = 1.92$ m. Davidson *et al.*
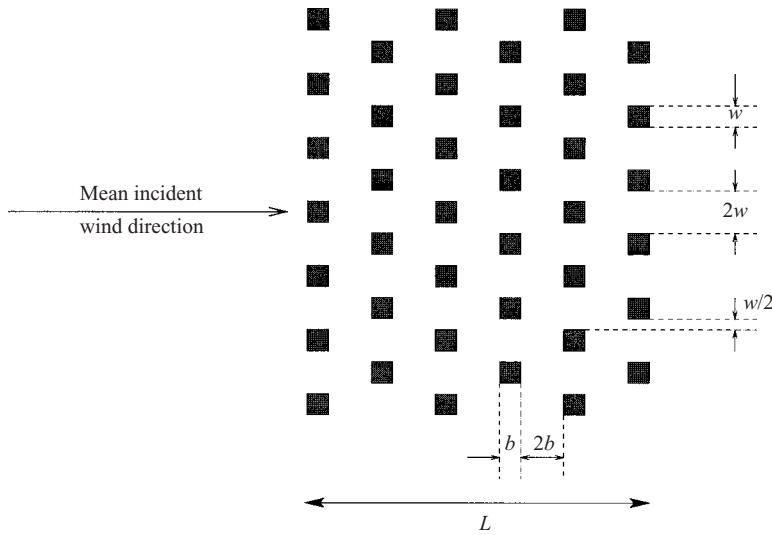
FIGURE 10. The obstacle layout in Davidson *et al.*'s (1995*a*) experiments.

	Height, h_e (m)	Length, L (m)	$L_c(\bar{c}_d = 3)$ (m)	$L_c(\bar{c}_d = 5)$ (m)
Field	2.3	44.1	14.8	8.9
Wind tunnel	0.12	1.92	0.72	0.43

TABLE 1. Parameters for the model calculations of the experiments of Davidson *et al.*

measured mean streamwise velocities at half the height of the buildings. For each fetch, the streamwise velocity was measured at a range of lateral positions. Davidson *et al.* then averaged these measurements to yield an estimate of the spatially averaged mean streamwise velocity, which are now compared with the values computed by the model. This procedure was repeated at a range of fetches to quantify the deceleration caused by the array. Assuming that lateral velocity gradients near the array centreline are negligible, so that the centreline flow can be described by the two-dimensional model, the measured velocities can be compared with predictions using the present distributed force model.

In both experiments the incident velocity profile was logarithmic, with roughness parameters $z_0 = 11\,\text{mm}$, $u_* = 0.49\,\text{m s}^{-1}$ (field) and $z_0 = 0.4\,\text{mm}$, $u_* = 0.21\,\text{m s}^{-1}$ (wind tunnel). The roughness density, $\lambda = N_e A_f / A_t$, for the experiments is $\lambda = (w_e \times h_e)/(3b_e \times 3w_e) = 0.1$, for both the field and wind-tunnel experiments. The fraction of volume occupied by fluid is $1 - \beta = 0.89$. Drag coefficients for the individual obstacles were not measured. Our calculations use two assumed values for the sectional drag coefficient: $\bar{c}_d = 3$ and $\bar{c}_d = 5$; this enables us to assess the dependence of wind deceleration on $\bar{c}_d$ as well as to see whether our range of predictions includes the experimental data. Values of the sectional drag coefficient, $\bar{c}_d$, are higher than values of the bulk drag coefficient, which is referenced to a velocity at the cube height. Nevertheless the values used here for $\bar{c}_d$ are higher than expected. We return to this question later. These parameters yield, on using (2.4) and $\lambda = 0.1$, the values of L_c shown in table 1. Thus, the obstacle canopies of the two experiments
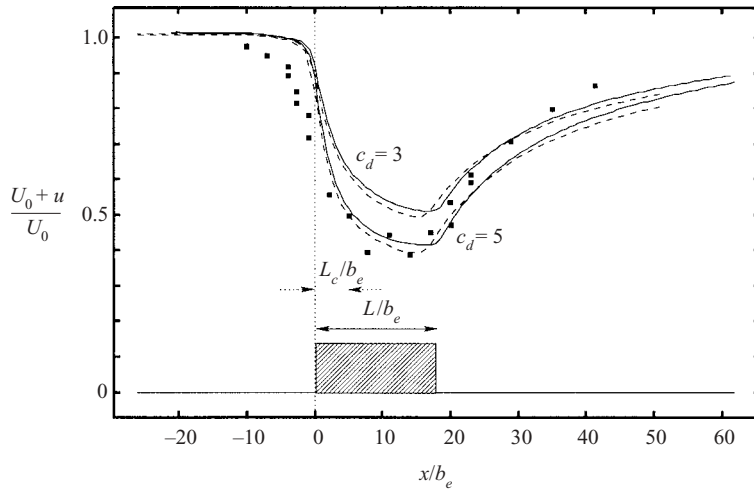
FIGURE 11. Deceleration of the mean wind $(U_0 + u)/U_0$ at $z = h_e/2$ through an obstacle canopy. Points: measurements of Davidson *et al.* (1995*a*,*b*). Solid lines: present theory with parameters for the field experiment. Dashed lines: present theory with parameters for the wind tunnel experiment. For each experimental configuration the theory is computed using the simple mixing length theory and for $\bar{c}_d = 3$ and 5.

are modelled by rectangular drag distributions with height, length and values of L_c given in table 1. Notice that in all cases $h_e/L_c \ll 1$ and $L_c/L \ll 1$, typical of urban areas.

The comparison is shown in figure 11. Note that, as shown by Davidson *et al.*, data from the two experiments collapse onto each other when non-dimensionalized as in figure 11. This is because the model and full scale roughness heights are in approximately the same ratio as the obstacle dimensions (as measured by the roughness density, λ). There is good agreement between theory and experiment in the overall form of the deceleration curve. In particular, the model correctly captures the magnitude of the significant reduction in wind speed through the canopy. Notice how the maximum velocity deficit is related nonlinearly to the drag coefficient $\bar{c}_d$.

Note the marked difference in the velocity reduction at the leading edge of the canopy in figure 11 compared to the plant canopies considered before. In the model computations, $(U_{h_e/2} + u(x = 0))/U_{h_e/2} \approx 0.9$, in agreement with (4.21). However, this does not agree with the measurements, which show a larger drop upwind at $x = 0$. The reason is that in this experiment the blocking effect by the large canopy elements is significant. At a distance $x = -(g_e + b_e) \approx -3b_e$, the deceleration from this blocking estimated from (4.22) is

$$\frac{U_{h_e/2} + u}{U_{h_e/2}} \sim 1 - \frac{b_e^2}{(g_e + b_e)^2} \approx 0.9 \quad \text{at} \quad \frac{x}{b_e} \approx -3, \tag{5.4}$$

which is in remarkably good agreement with the measured value. This blocking mechanism acts additively to the drag mechanism. Hence, it seems likely that a quantitative model with both mechanisms represented would yield good agreement with the data with a smaller, and more plausible, value of $\bar{c}_d$.

Notice also that the velocity deficit recovers more quickly downwind than in the linear distributed force model because of the neglect of the nonlinear inertial forces. The quasi-linear model is clearly able to capture well the deceleration in the canopy.

This comparison therefore shows, for the first time, that a canopy approach can be used to model quantitatively the spatially averaged flow in a group of large obstacles.

6. Variation of the effective roughness of the canopy

The flow above the canopy can be modelled by representing the canopy as a roughness, with effective roughness length, z_0^{eff}, and effective displacement height, d^{eff} (although this approach does not resolve the detailed dynamics of the canopy described by the present model). As we shall now see, these effective parameters vary with fetch through the adjustment region.

When the internal boundary layer above the canopy has grown sufficiently, the mean velocity just above the canopy takes the form

$$U(x, z) = \frac{u_*^{eff}(x)}{\kappa} \ln \left(\frac{z - d^{eff}(x)}{z_0^{eff}(x)} \right). \tag{6.1}$$

The effective parameters that govern the canopy can be deduced from the linear analytical model described above as follows. First, the linear perturbation to the wind profile caused by the canopy, u, becomes, on neglecting products of perturbations,

$$u(x, z) = U(x, z) - U_0(z) = \frac{(u_*^{eff} - u_*)}{\kappa} \ln(z/z_0) - \frac{u_*}{\kappa} M^{eff} - \frac{u_*}{\kappa z} d^{eff}. \tag{6.2}$$

Here, $M^{eff} = \ln(z_0^{eff}/z_0)$ and u_* is the friction velocity in the incident flow. Sufficiently far along the canopy, $x \gg L_c$, $M^{eff} = M_\infty^{eff}$. The difference between M^{eff} and M_∞^{eff} is caused by the changing flow in the adjustment region of figure 3.

The three terms on the right-hand side of (6.2) describe perturbations to the friction velocity, roughness length and displacement height. The effective parameters can then be obtained by first calculating the Fourier transform of (6.2), which yields

$$\tilde{u}(k, z) = \frac{\tilde{\tau}(k)}{2\kappa u_*} \ln\{(z - d)/z_0\} - \frac{u_*}{\kappa} \tilde{M}^{eff} - \frac{u_*}{\kappa z} \tilde{d}^{eff}, \tag{6.3}$$

and then by comparing with the linear solution calculated in §4 (see Jerram 1995, §5.2 for details). When the displaced mixing-length model is used, this procedure leads to

$$M^{eff}(x) = \frac{1}{2u_*^2} \int_{z_c}^\infty f(x, z') \ln \left(\frac{z' - d}{z_0} \right) dz' - \frac{u_c}{u_*}, \tag{6.4}$$

$$d^{eff}(x) = d. \tag{6.5}$$

Thus, the varying effective roughness length $M^{eff}(x)$ has two components: first, a step change associated with the step change in the canopy drag; and secondly a positive, and comparable, contribution associated with the variation in the slip velocity, $u_c(x)$, at the height z_c within the canopy where the mixing-length changes from being constant with height to varying linearly with height. $M^{eff}(x)$ rises to its equilibrium value over a distance of order L_c. In classical roughness change experiments (e.g. Bradley 1968), this length corresponds to a few, perhaps, 4 or 5, obstacle heights. The effective displacement height remains the origin of the mixing length above the canopy, i.e. d for the displaced mixing-length model.

The results for the effective parameters for the standard mixing-length model are obtained by setting $z_c = z_0$, $d = 0$ and $u_c = 0$. The effective roughness length with the standard mixing-length model is larger than with the displaced mixing-length
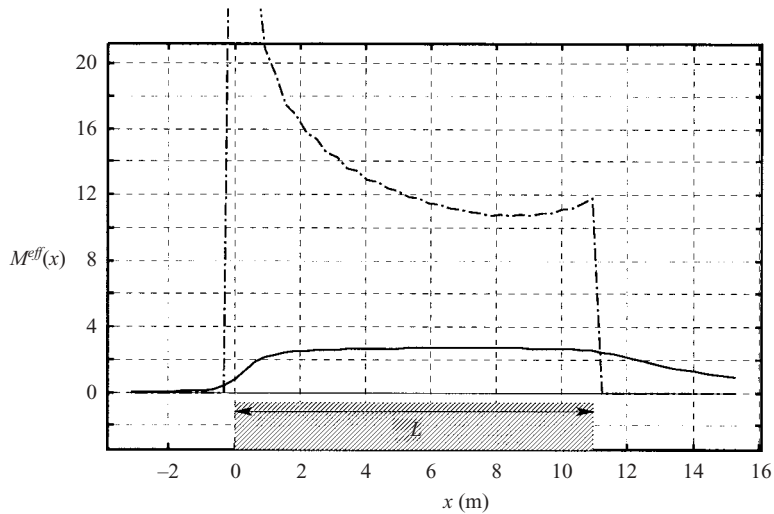
FIGURE 12. Variation of the effective roughness length parameter $M^{eff}(x) = \ln(z_0^{eff}/z_0)$ with fetch. Dot-dashed line: present theory with the simple mixing-length model. Solid line: present theory with the displaced mixing-length model. The parameters are as for the simulations of Meroney's (1968) experiment and the position of the canopy is denoted by the hatched area.

model (since explicit computations show that u_c is positive). The displacement height remains zero when the standard mixing-length is used.

The variation of $M^{eff}(x)$ with fetch for the parameters used in §5.2 for Meroney's laboratory experiments is shown in figure 12. With the displaced mixing-length model, an equilibrium value of M^{eff} of about 2.7, which corresponds to an effective roughness length of 2.6 cm, is reached after a fetch of about 1 m. This value can be compared with a value obtained from the wind profile over the same model canopy measured by Hsi & Nath (1970). When their measurements are replotted, the displacement height can be inferred, following Thom (1971) and Jackson (1981), from the level of mean momentum absorption, and is found to be $d = 12.6$ cm. A good fit to the measured wind profile is then obtained with an effective roughness length of 1.6 cm, which is in reasonable agreement with the value 2.6 cm calculated here. The effective roughness length depends only weakly on the values of the other parameters in the displaced mixing-length model.

The value of the effective roughness length obtained from the model with the standard mixing-length model, however, is very much larger – too large to be credible. This error occurs because the standard mixing-length model yields a zero displacement height.

For the Meroney experiment, the effective roughness length reaches its equilibrium value approximately 1 m into the canopy. This distance corresponds to about $7L_c$. For shorter fetches, the effective roughness length makes a transition from its small value upstream. Downstream of the canopy, the effective roughness length adjusts to its upstream value, but more slowly than the adjustment within the canopy.

This method provides a systematic way of estimating the effective roughness length over a canopy in terms of its drag distribution $f(x, z)$ and may improve current approximate methods. The results within the adjustment region differ from the estimates for z_0^{eff} derived by Thom (1971) and Jackson (1981) because they did not consider the loss of momentum in the boundary layer produced by the efflux out of the top of the canopy.

The variation in this adjustment region should be incorporated into numerical weather prediction models which currently assume (e.g. Wood & Mason 1993; Goode & Belcher 1999) (i) that the surface drag is parameterized by z_0 defined on an appropriate computational mesh, (ii) that the near surface flow adjusts immediately to any changes in roughness and (iii) that the flow passes over the top of the canopy. The second assumption partly compensates for the third. However, these approximate methods do not account for the high drag in the adjustment region.

7. Conclusions

A general approach has been developed for understanding how deep turbulent boundary layers adjust as they flow over and through a canopy of roughness elements. Following work on plant canopies, mean momentum equations are obtained by averaging both temporally and spatially. These mean flow equations contain two new terms: (i) the drag that arises from averaging spatially the form drag due to individual canopy elements; and (ii) a finite-volume effect whereby momentum is transported by displacement of streamlines around individual canopy elements. The present study has focused on the case when the fraction of volume occupied by the roughness elements, β, is small. Over the bulk of the flow, the drag of the canopy elements is the dominant process. In the impact region, just upstream of the canopy, however, the finite volume effect is large when the canopy elements are large.

Scaling arguments have identified three stages of the adjustment. First, the drag and the finite volumes of the canopy elements decelerate air parcels; the associated pressure gradient decelerates the flow within an *impact region* upwind of the canopy. Secondly, within an *adjustment region* of length of order L_c downwind of the leading edge of the canopy, the flow within the canopy decelerates substantially until it comes into a local balance between downward transport of momentum by turbulent stresses and removal of momentum by the drag of the canopy elements. The adjustment length, L_c, is proportional to (i) the reciprocal of the roughness density (defined to be the frontal area of canopy elements per unit floor area) and (ii) the drag coefficient of individual canopy elements. Further downstream, within a *roughness-change region*, the canopy is shown to affect the flow above as if it were a change in roughness length, leading to the development of an internal boundary layer.

A quantitative model for the adjustment of the flow is developed by calculating analytically small perturbations to a logarithmic velocity profile induced by the drag due to a sparse canopy with $L/L_c \ll 1$, where L is the length of the canopy. These linearized solutions are then evaluated numerically with a nonlinear correction to account for the drag varying with the velocity. A further correction is derived to account for the finite volume of the canopy elements.

The results are shown to compare well with experimental measurements in a fine-scale vegetation canopy, when the drag is more important than the finite-volume effects, and a canopy of coarse-scale cuboids, when the finite-volume effects are of comparable importance to the drag in the impact region.

An expression is derived showing how the effective roughness length of the canopy, z_0^{eff}, is related to the drag in the canopy. The value of z_0^{eff} varies smoothly with fetch through the adjustment region from the roughness length of the upstream surface to the equilibrium roughness length of the canopy. Hence, the analysis shows how to resolve the unphysical flow singularities obtained with previous models of flow over sudden changes in surface roughness.

Finally, we note that the method of this paper can be applied to the changes in scalar fields associated with large roughness changes, using the methods developed

by Raupach (1992) and Hewer & Wood (1998) together with the concept of an adjustment region developed here.

REFERENCES

ABRAMOWITZ, M. & STEGUN, I. A. 1972 *Handbook of Mathematical Functions*. Dover.

AYOTTE, K. W., FINNIGAN, J. J. & RAUPACH, M. R. 1999 A second-order closure for neutrally stratified vegetative canopy flows. *Boundary-Layer Met.* **90**, 189–216.

BATCHELOR, G. K. 1967 *An Introduction to Fluid Dynamics*. Cambridge University Press.

BELCHER, S. E. & HUNT, J. C. R. 1998 Turbulent air flow over hills and waves. *Annu. Rev. Fluid Mech.* **30**, 507–538.

BELCHER, S. E., NEWLEY, T. M. J. & HUNT, J. C. R. 1993 The drag on an undulating surface induced by the flow of a turbulent boundary layer. *J. Fluid Mech.* **249**, 557–596.

BELCHER, S. E., XU, D. P. & HUNT, J. C. R. 1990 The response of a turbulent boundary layer to arbitrarily distributed two-dimensional roughness changes. *Q. J. R. Met. Soc.* **116**, 611–635.

BOHM, M., FINNIGAN, J. J. & RAUPACH, M. R. 2000 Dispersive fluxes in canopy flows: just how important are they? *Proc. 24th Conf. on Agricultural and Forest Meteorology, American Meteorological Society, Davis, CA, August 2000.*

BRADLEY, E. F. 1968 A micrometeorological study of velocity profiles and surface drag in the region modified by a change in roughness. *Q. J. R. Met. Soc.* **94**, 361–379.

BRITTER, R. E. & HUNT, J. C. R. 1979 Velocity measurements and order-of-magnitude estimates of the flow between two buildings in a simulated atmospheric boundary. *J. Indust. Aerodyn.* **4**, 165–182.

CHENG, H. & CASTRO, I. P. 2002*a* Near wall flow over urban like roughness. *Boundary-Layer Met.* **104**, 229–259.

CHENG, H. & CASTRO, I. P. 2002*b* Near-wall flow development after a step change in surface roughness. *Boundary-Layer Met.* **105**, 411–432.

COUNIHAN, J., HUNT, J. C. R. & JACKSON, P. S. 1974 Wakes behind two-dimensional obstacles in turbulent boundary layers. *J. Fluid Mech.* **64**, 529–563.

DAVIDSON, M. J., MYLNE, K., MOLYNEUX, M., JONES, C. D., PERKINS, R. J. & HUNT, J. C. R. 1995*a* Plume dispersion through large groups of obstacles – a field investigation. *Atmos. Environ.* **29**, 3245–3256.

DAVIDSON, M. J., SNYDER, W. H., LAWSON, R. E. & HUNT, J. C. R. 1995*b* Plume dispersion from point sources upwind of groups of obstacles – wind tunnel simulations. *Atmos. Environ.* **30**, 3245–3731.

EAMES, I., HUNT, J. C. R. & BELCHER, S. E. 2003 Eulerian and Lagrangian analysis of flow through groups of obstacles. *J. Fluid Mech.* (submitted).

FINNIGAN, J. J. 1985 Turbulent transport in flexible plant canopies. In *The Forest–Atmosphere Interaction* (ed. B. A. Hutchinson & B. B. Hicks), pp. 443–480. Reidel.

FINNIGAN, J. J. 2000 Turbulence in plant canopies. *Annu. Rev. Fluid Mech.* **32**, 519–571.

FINNIGAN, J. J. & BELCHER, S. E. 2003 Flow over a hill covered with a plant canopy. *Q. J. R. Met. Soc.* (to appear).

FINNIGAN, J. J. & BRUNET, Y. 1995 Turbulent air flow in forests on flat and hilly terrain. In *The Forest–Atmosphere Interaction* (ed. B. A. Hutchinson & B. B. Hicks), pp. 443–480. Reidel.

GOODE, K. & BELCHER, S. E. 1999 On the parameterisation of the effective roughness length for momentum transfer over heterogeneous terrain. *Boundary-Layer Met.* **93**, 133–154.

GRIMMOND, C. S. B. & OKE, T. R. 1999 Aerodynamic properties of urban areas derived, from analysis of surface form. *J. Appl. Met.* **38**, 1262–1292.

HEWER, F. E. & WOOD, N. 1998 The effective roughness length for scaler transfer in neutral conditions over hilly terrain. *Q. J. R. Met. Soc.* **124**, 659–685.

Hsi, G. & Nath, J. H. 1970 Wind drag within simulated forest canopies. *J. Appl. Met.* **9**, 592–602.

Hunt, J. C. R. & Durbin, P. A. 1999 Perturbed vortical layers and shear sheltering. *Fluid Dyn. Res.* **24**, 375–404.

Hunt, J. C. R., Leibovich, S. & Richards, K. J. 1988 Turbulent shear flow over low hills. *Q. J. R. Met. Soc.* **114**, 1435–1471.

Hunt, J. C. R., Sandham, N. D., Vassilicos, J. C., *et al.* 2001 Developments in turbulence research: a review based on the 1999 Programme of the Isaac Newton Institute, Cambridge. *J. Fluid Mech.* **436**, 353–391.

Inoue, E. 1963 On the turbulent structure of airflow within crop canopies. *J. Met. Soc. Japan* **49**, 121–124.

Jackson, P. S. 1981 On the displacement height in the logarithmic velocity profile. *J. Fluid Mech.* **111**, 15–25.

Jackson, P. S. & Hunt, J. C. R. 1975 Turbulent wind flow over a low hill. *Q. J. R. Met. Soc.* **101**, 929–955.

Jerram, N. 1995 Turbulent flow and dispersion through groups of obstacles. PhD thesis, University of Cambridge.

Kaimal, J. C. & Finnigan, J. J. 1995 *Atmospheric Boundary Layer Flows*. Oxford University Press.

Kowe, R., Hunt, J. C. R., Hunt, A., Couet, B. & Bradbury, L. S. J. 1988 The effect of bubbles on the volume fluxes and the presure gradients in non-uniform steady flow of liquids. *Intl J. Multiphase Flow* **14**, 587–606.

Krettenauer, K. & Schumann, U. 1992 Numerical simulation of turbulent convection over wavy terrain. *J. Fluid Mech.* **237**, 261–299.

Louka, P., Belcher, S. E. & Harrison, R. G. 2000 Coupling between air flow in streets and the well-developed boundary layer aloft. *Atmos. Environ.* **34**, 2613–2621.

MacDonald, R. W. 2000 Modelling the mean velocity profile in the urban canoyp layer. *Boundary-Layer Met.* **97**, 25–45.

Mayhead, G. J., Gardiner, J. B. H. & Durrant, D. W. 1975 Physical properties of conifers in relation to plantation stability. Unpublished report, Forestry Commission, Edinburgh.

Meroney, R. N. 1968 Characteristics of wind and turbulence in and above model forests. *J. Appl. Met.* **7**, 780–788.

Raupach, M. R. 1992 Drag and drag partition on rough surfaces. *Boundary-Layer Met.* **60**, 375–395.

Raupach, M. R., Finnigan, J. J. & Brunet, Y. 1996 Coherent eddies and turbulence in vegetation canopies: the mixing layer analogy. *Boundary-Layer Met.* **78**, 351–382.

Raupach, M. R. & Shaw, R. H. 1982 Averaging procedures for flow within vegetation canopies. *Boundary-Layer Met.* **22**, 79–90.

Raupach, M. R., Thom, A. S. & Edwards, I. 1980 A wind-tunnel study of turbulent flow close to regularly arrayed rough surfaces. *Boundary-Layer Met.* **18**, 373–397.

Rotach, M. W. 1993 Turbulence close to a rough urban surface. Part I: Reynolds stress. *Boundary-Layer Met.* **65**, 1–28.

Stacey, G. R., Belcher, R. E., Wood, C. J. & Gardiner, B. A. 1994 Wind flows and forces in a model spruce forest. *Boundary-Layer Met.* **69**, 311–334.

Svensson, U. & Häggkvist, K. H. 1990 A two-equation turbulence model for canopy flows. *J. Wind Engng Indust. Aerodyn.* **35**, 201–211.

Taylor, G. I. 1944 Air resistance of a flat plate of very porous material. *Rep. Mem. Aero. Res. Council*, **2236**. [See also G. I. Taylor Scientific Papers (ed. G. K. Batchelor), vol. 3, pp. 383–386, Cambridge University Press (1963).]

Thom, A. S. 1971 Momentum absorption by vegetation. *Q. J. R. Met. Soc.* **97**, 414–428.

Townsend, A. A. 1965 Equilibrium layers and wall turbulence. *J. Fluid Mech.* **11**, 414–428.

Townsend, A. A. 1976 *The Structure of Turbulent Shear Flow*, 2nd edn. Cambridge University Press.

Wilson, J. D., Finnigan, J. J. & Raupach, M. R. 1998 A first order closure for disturbed plant canopy flows and its application to flow over a ridge. *Q. J. R. Met. Soc.* **124**, 705–732.

Wood, N. & Mason, P. J. 1993 The pressure force induced by neutral, turbulent flow over hills. *Q. J. R. Met. Soc.* **119**, 1233–1267.

Wooding, R. A., Bradley, E. F. & Marshall, J. K. 1973 Drag due to regular arrays of roughness elements. *Boundary-Layer Met.* **5**, 285–308.